Letter of Intent

Search for Missing Resonances in Photoproduction of Vector Mesons using a Polarized Photon Beam and a Polarized Target

F. Klein[1], D. Sober[1], H. Crannell[1], K. Livingston[2], U. Thoma[3], P. Cole[4]

[1] The Catholic University of America, Washington, DC 20064
[2] University of Glasgow, G12 8QQ, Glasgow, United Kingdom
[3] Jefferson Lab, Newport News, VA 23606
[4] University of Texas at El Paso, El Paso, TX 79968

Abstract

We propose to measure polarization observables for vector meson photoproduction using longitudinally and transversely polarized targets. This experiment is an extension of the approved experiments E94-109 and E99-013 (ρ and ω photoproduction using a linearly polarized photon beam) which, additionally, will use circularly polarized photons as probe in order to have access to the corresponding double polarization observables. Together with the polarization state of the photon-beam and the longitudinal/transverse polarization of the target-protons we will determine the tensor polarization of the vector mesons via analysis of the angular distribution of their decay particles. Calculations based on relativized quark models clearly show the importance of spin observables in the effort to disentangle various reaction mechanisms, especially s-channel processes involving N^* and Δ^*-states.

1 Introduction

We propose to measure polarization observables for the photoproduction of ρ and ω mesons using a polarized target in combination with beams of polarized photons. The measurement of the angular distributions of the decay products of these vector mesons will provide crucial information for the extraction of masses, partial widths, and helicity amplitudes of baryon resonances that decay via ρN or ωN. Due to the narrow decay width (8.43 MeV) of the ω meson and because of isospin selectivity, the ω meson channel will serve as an unique signal for extracting N^* resonances that possess an isospin of 1/2. The analysis of the reactions $\rho^0 p$ and $\rho^+ n$ will give us further information about Δ^* resonances ($I = \frac{3}{2}$) that decay into ρN. The latter reactions require the simultaneous analysis of the $\Delta\pi$ channels having the same final state as the ρN channels. Due to the large widths of ρ and Δ, those channels share the same kinematical regime ($p\pi\pi$ phase space).

By using CLAS, the photon tagger, and a continuous electron beam, we will be able to perform these measurements with large angular coverage, small systematic uncertainties, and high statistics.

Whereas diffractive and t-channel exchange contributions will dominate the ρ^0 and ω cross section at low t, and u-channel exchange will be large at high t, we expect the contributions from resonance production to be enhanced in the mid-t regime. The low- and high-t processes are of interest in their own right, and interference effects with resonant vector meson photoproduction may well be significant. We will be measuring over a large kinematical range in t, and thus will be sensitive to all of these processes. Furthermore, polarized photons in combination with a polarized target provide a powerful tool for disentangling the contributions of natural-parity (Pomeron, σ, f_2) and unnatural-parity exchange (mostly pion) in the t-channel.

2 Motivation

The spectrum of excited states of a system of bound particles opens a window to the underlying interaction. Just as in nuclear spectroscopy, where the spectrum of excited states reflects the quantum many-body configurations of nucleons and mesons interacting via the strong nuclear force, so does baryon spectroscopy afford us the opportunity to study the interaction of quarks and gluons in excited states.

An important motivation for studying the spectrum of baryon resonances with photons is to obtain information on the photoproduction amplitudes of the individual resonances. Most of our knowledge of the baryon resonance spectrum has come from the reactions $\pi N \to \pi N$, $\gamma N \to \pi N$, and $\pi N \to \pi\pi N$. At center-of-mass energies below 1.7 GeV, the single pion production channel dominates both the pion and photoabsorption cross sections. As the c.m. energy increases towards 2.0 GeV, the two- and three-pion decay channels become dominant, and it is in this energy region that the masses and partial widths of the resonances are poorly determined.

An outstanding problem in our understanding of baryon spectroscopy is that of the missing resonances. For example, SU(6) $\otimes$ O(3) symmetric quark models predict far more resonances than have been observed. One solution is to restrict the number of internal degrees of freedom by assuming that two quarks are bound in a diquark pair [1], thus lowering the level density of baryon resonances. An alternate solution has been put forward by Koniuk and Isgur [2] and others [3, 4]. In these calculations, it was found that the missing resonances tend to couple weakly to the πN channel but more strongly to the ρN, $\Delta\pi$, and ωN channels. For example, in Table 1, we tabulate the supermultiplet assignments with the corresponding PDG [8] star rating for the measured and missing baryon resonances from the QCD-improved model of Cutkosky [9]. The supermultiplets in the boxes are fully consistent with the predictions of the diquark model. All of the boxed entries have at least a three-star rating. We remark that the positive parity P11(1710) and P13(1870) resonances are inconsistent with the diquark model. The partial widths for the photon and hadronic couplings in the Koniuk-Isgur framework are contained in Table 2. We note that the P13(1870) as well as the F15(1955) are predicted to have primarily an ωN decay mode. Since most of our information on the baryon resonance spectrum comes from partial-wave analyses of $\pi N \to \pi N$ measurements, these 'missing states' clearly have escaped detection. The models predict that these resonances have a reasonable coupling to the photon. We expect the identification of many of these resonances decaying through the ρN and ωN modes to be difficult due to their broad widths and narrow spacing. The sensitivity afforded by linearly and circularly polarized photons together with longitudinally and transversely polarized targets will provide most powerful constraints in identifying these resonances.

Experimentally, several difficulties are apparent. The number of resonances extracted either from the analyses of pion production data or from the theoretical predictions is large. In addition, the resonance widths are broad (typically $\sim$ 150 MeV), and one is faced with the problem of disentangling many overlapping resonances. Moreover, diffraction-like processes dominate the vector meson photoproduction at forward angles. A phase-shift analysis is required to identify resonant behavior, and to extract the helicity amplitudes for the various resonances. Such an analysis is greatly aided by the measurement of polarization observables.

Table 1: SU(6) $\otimes$ O(3) supermultiplet assignments from the QCD-improved model of Cutkosky for the measured and *missing* baryon resonances. The boxed supermultiplets are fully consistent with the diquark model.

N^*	Status	SU(6) $\otimes$ O(3)	Parity	Δ^*	Status	SU(6) $\otimes$ O(3)
P11(938)	****	$\boxed{(56,0^+)}$	$+$	P33(1232)	****	$\boxed{(56,0^+)}$
S11(1535)	****	$\boxed{(70,1^-)}$				
S11(1650)	****	$\boxed{(70,1^-)}$		S31(1620)	****	$\boxed{(70,1^-)}$
D13(1520)	****	$\boxed{(70,1^-)}$	$-$	D33(1700)	****	$\boxed{(70,1^-)}$
D13(1700)	***	$\boxed{(70,1^-)}$				
D15(1675)	****	$\boxed{(70,1^-)}$				
P11(1520)	****	$\boxed{(56,0^+)}$		P31(1875)	****	$\boxed{(56,2^+)}$
P11(1710)	***	$(70,0^+)$		P31(1835)		$(70,0^+)$
P11(1880)		$(70,2^+)$				
P11(1975)		$(20,1^+)$				
P13(1720)	****	$\boxed{(56,2^+)}$		P33(1600)	***	$\boxed{(56,0^+)}$
P13(1870)	*	$(70,0^+)$		P33(1920)	***	$\boxed{(56,2^+)}$
P13(1910)		$(70,2^+)$	$+$	P33(1985)		$(70,2^+)$
P13(1950)		$(70,2^+)$				
P13(2030)		$(20,1^+)$				
F15(1680)	****	$\boxed{(56,2^+)}$		F35(1905)	****	$\boxed{(56,2^+)}$
F15(2000)	**	$(70,2^+)$		F35(2000)	**	$(70,2^+)$
F15(1995)		$(70,2^+)$				
F17(1990)	**	$(70,2^+)$		F37(1950)	****	$\boxed{(56,2^+)}$

Table 2: Partial widths for photon and hadronic couplings to baryon resonances in the Isgur-Karl model. The total hadronic width, summed over all identified channels, is also given. The units are MeV.

Mass	J^π	γp	πN	$\pi\Delta$	ρN	ωN	Total
N(1490)	$1/2^-$	1.3	28.	2.9	40.	0.	98.
N(1655)	$1/2^-$	0.72	76.	67.	102.	1.4	262.
N(1535)	$1/2^-$	0.58	85.	52.	27.	0.	164.
N(1745)	$3/2^-$	0.009	13.	317.	26.	2.9	360.
N(1670)	$5/2^-$	0.013	30.	86.	5.3	0.	130.
N(1405)	$1/2^+$	0.026	46.	5.8	0.1	0.	52.
N(1705)	$1/2^+$	0.23	45.	13.	36.	0.8	108.
N(1890)	$1/2^+$	0.057	19.	12.	22.	37.	96.
N(2055)	$1/2^+$	0.009	1.4	3.2	1.7	32.	39.
N(1710)	$1/2^+$	1.0	42.	4.4	156.	32.	242.
N(1870)	$3/2^+$	0.027	10.	19.	2.3	98.	149.
N(1955)	$3/2^+$	0.021	1.2	88.	56.	90.	236.
N(1980)	$3/2^+$	0.031	1.2	96.	71.	55.	223.
N(2060)	$3/2^+$	0.0001	0.3	31.	15.	98.	145.
N(1715)	$5/2^+$	0.29	50.	4.4	20.	1.4	77.
N(1955)	$5/2^+$	0.24	0.2	64.	67.	184.	324.
N(2025)	$5/2^+$	0.001	1.7	67.	66.	180.	316.
N(1955)	$7/2^+$	0.006	9.6	36.	18.	53.	126.
Δ(1685)	$1/2^-$	0.34	11.	64.	64.	−−	139.
Δ(1685)	$3/2^-$	1.0	24.	146.	289.	−−	459.
Δ(1925)	$1/2^+$	0.0	28.	35.	37.	−−	112.
Δ(1240)	$3/2^+$	0.46	121.	0.	0.	−−	121.
Δ(1780)	$3/2^+$	0.14	29.	74.	32.	−−	139.
Δ(1975)	$3/2^+$	0.030	0.	59.	35.	−−	94.
Δ(1940)	$5/2^+$	0.059	16.	41.	45.	−−	103.
Δ(1975)	$5/2^+$	0.51	1.	41.	388.	−−	430.
Δ(1915)	$7/2^+$	0.27	56.	30.	88.	−−	178.

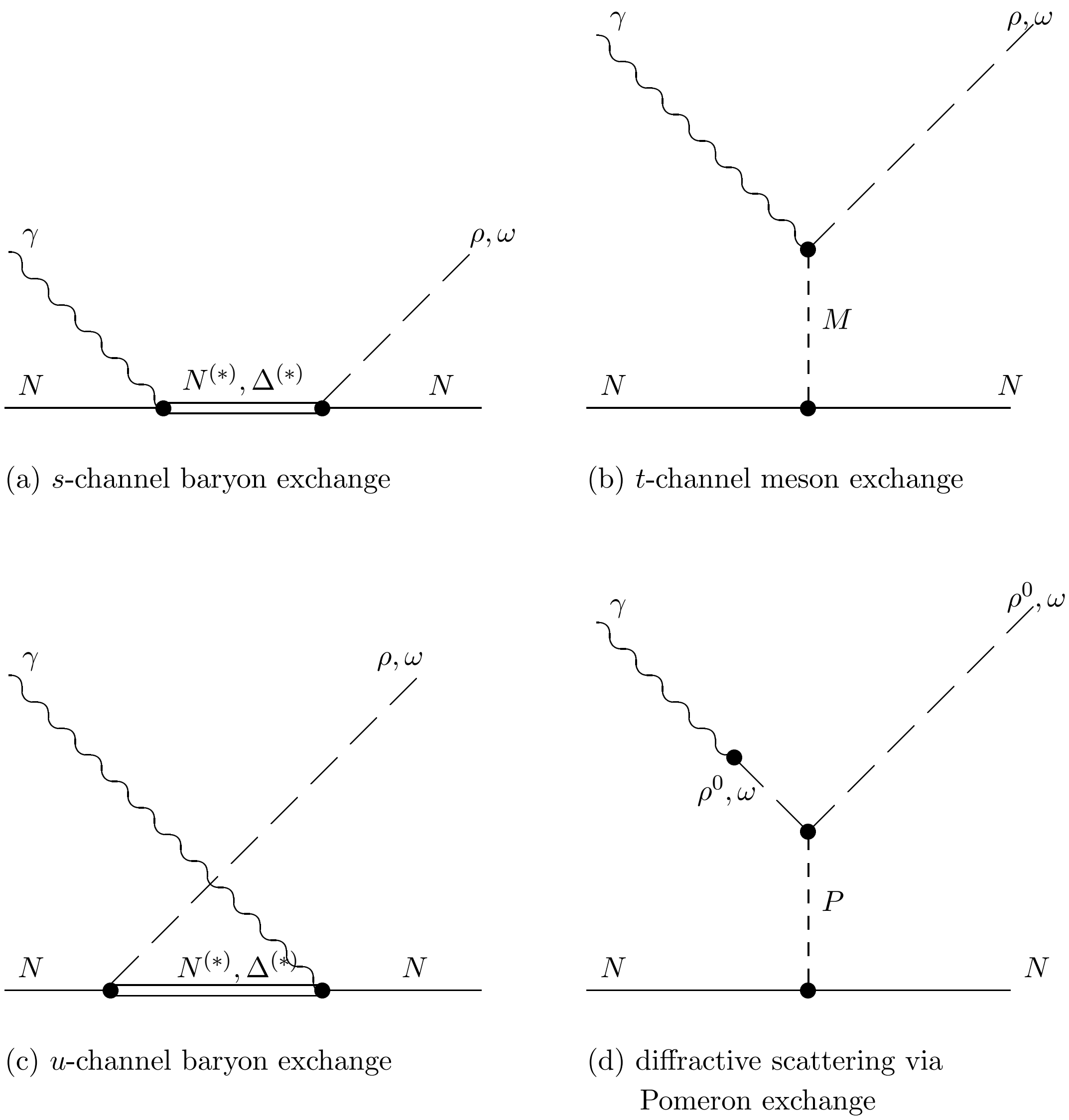

(a) s-channel baryon exchange

(b) t-channel meson exchange

(c) u-channel baryon exchange

(d) diffractive scattering via Pomeron exchange

Figure 1: Processes involved in ρ and ω-meson photoproduction.

3 Production dynamics

3.1 Processes contributing to ρ and ω photoproduction

From the duality principle, the cross section for ρ and ω photoproduction can be calculated, in principle, by summing over all possible t-channel meson-exchange processes [Fig. 1(b)], or over all possible s-channel *plus* all possible u-channel baryon-exchange processes. The pomeron exchange contribution to diffractive scattering of Fig. 1(d) needs to be added as a special case, as the effects of pomeron exchange in the t-channel are understood to be in addition to those of meson exchange. In the diffractive (low-t) region, it is more efficient to sum over t-channel exchange processes, as the sum over s-channel plus u-channel processes would require a large number of intermediate baryon states for convergence. Similarly, in the resonance region a t-channel sum will yield only the average cross section and will not show the characteristic energy dependence attributed to baryon resonances.

Constructing the cross section from a model, and likewise extracting resonance parameters from an analysis of the cross section, will therefore require different approaches in different kinematical regions. The s-channel sum used for an estimate of the resonance region cross section needs to be supplemented by the terms representing the u-channel diagrams of Fig. 1(c).

3.2 Model predictions

Our current calculations[1] are based on the constituent quark model approach by Q. Zhao, Z.P. Li, and C. Bennhold [15]; using an effective Lagrangian approach, the interaction between a vector meson[2] and the quarks inside the baryon is described within the SU(6) $\otimes$ O(3) symmetry limit. It further takes into account t-channel exchange mechanisms, which dominate in the low-t range: σ-exchange ($J^\pi = 0^+$) in ρ^0 production and π^0-exchange ($J^\pi = 0^-$) in ω production.

In the s-channel, the helicity amplitudes of all contributing baryons below 2 GeV (cf. Table 1) are calculated separately, and the excited states at higher masses are treated as degenerate in that scant information is available on these higher baryon resonances. The u-channel contributions include all baryonic states which are treated as degenerate, except the nucleon-exchange for all channels and the Δ-exchange in ρ production.

The calculations show that the partial widths of those resonances decaying into ωN and the

[1] We will include predictions of the model by Y. Oh and H.S. Lee which incorporates the quark model calculations by S. Capstick and W. Roberts in the proposal.

[2] The vector meson is treated as point-like particle in this model.

photon helicity amplitudes $A_{\frac{1}{2}}, A_{\frac{3}{2}}$ are consistent with the theoretical results of the NRQM approach in Ref. [2]. $P_{13}(1910)$ and $F_{15}(2000)$ have the largest decay widths into ωN ($\sqrt{\Gamma_\omega}$=1.38 MeV$^{-1/2}$ and 2.64 MeV$^{-1/2}$) – these results differ from the $^3P_0$ quark model of S. Capstick and W. Roberts [5] in which the $P_{13}(1910)$ possesses the largest decay width in $\gamma p \to \omega p$.

Contributions to the differential cross section and beam asymmetry for $\gamma p \to \omega p$ were shown in the proposal for omega production using linearly polarized photons [23]. We recall that s-channel contributions of individual resonances could not be disentangled by a measurement of the differential cross section alone. Predictions on the evolution of the density matrix elements as functions of E_{cm} and θ_{cm} were also plotted in this proposal. These observables were found to be more sensitive to contributions of specific resonances than the differential cross section. They describe combinations of beam asymmetry parameters and tensor polarization quantities of the vector meson.[3]

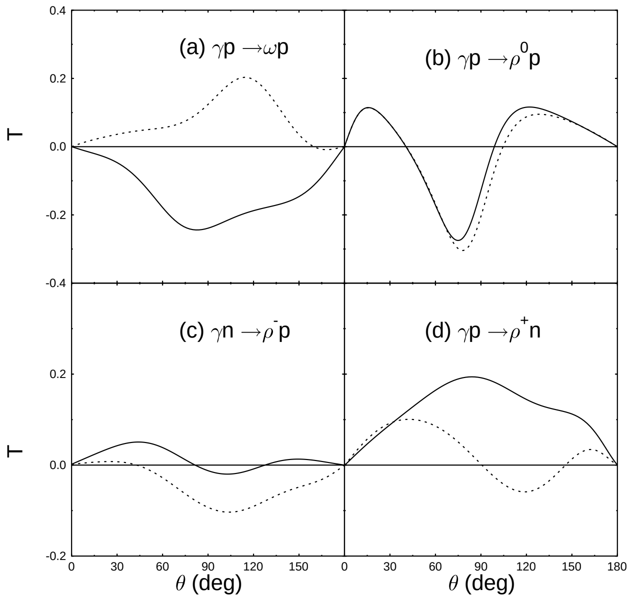

Figure 2: Target polarization (T_y) for vector meson photoproduction at E_γ = 1.9 GeV in the framework of the quark model approach by Z. Qiao, Z.P. Li, and C. Bennhold: the *solid* line represents $T_y(\theta_V)$ for t-channel exchange and all involved baryonic states which are taken into consideration in this model; the *dashed* line shows the same calculation but without the 'missing' resonance $F_{15}(2000)$. The most sensitive reaction channels are obviously $\gamma\vec{p} \to \omega p$ and $\gamma\vec{p} \to \rho^+ n$.

Crucial additional information has to be extracted from other polarization observables, especially those involving polarized targets. As an example, the target asymmetry is shown in Fig. 2 for a specific energy (E_γ = 1.9 GeV) where the *solid* curves describe the coherent sum of t-channel exchange (π, σ) and all contributions of baryon resonances (in s- and u-channels) whereas the *dashed*

[3]We refer the reader to the appendix which contains a short summary of helicity formalism, spin matrices, and polarization observables.

curves represent the coherent sum of the same contributions except $F_{15}(2000)$. The graphs show the sensitivity of the target asymmetry for ω and all ρ channels. According to this model, ωp as well as $\rho^+ n$ are most sensitive to contributions of this baryonic resonant state.

Nevertheless, due to the large contribution of t-channel processes in the photoproduction of vector mesons, an unambiguous distinction of individual resonance formation is only expected in case that a small number of baryonic resonances couple strongly to the vector meson channels. It is crucial to combine measurements with linearly and circularly polarized photon beam as well as longitudinally and transversely polarized targets. Especially those polarization observables are of great interest which vanish for t-channel exchanges.

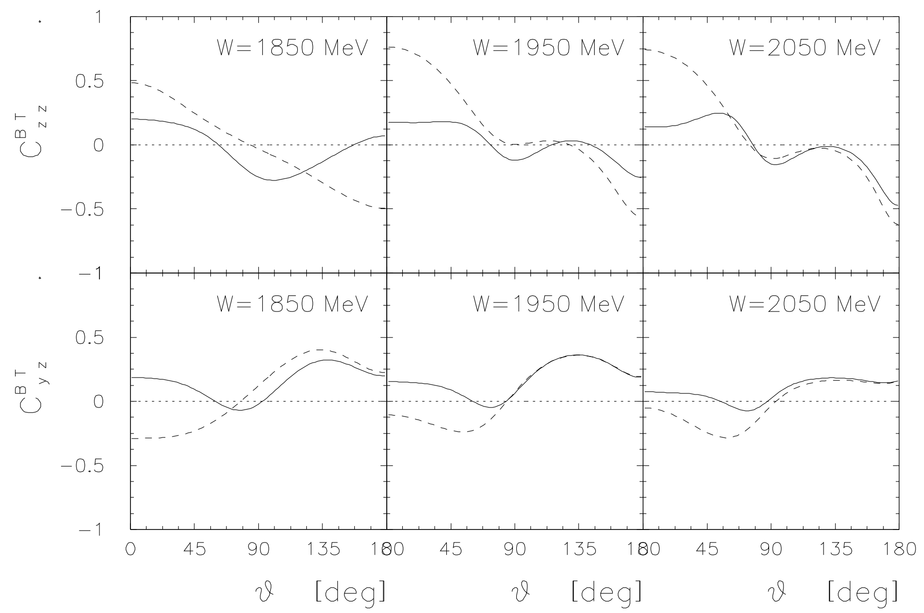

Figure 3: Beam–Target double polarization observables in $\gamma p \to \omega p$ for longitudinally polarized target in combination with circularly (*top*) and linearly (*bottom*) polarized photon beams. The *dashed* line shows the contribution from π-exchange. The *solid* line shows the predictions for the C^{BT} terms if all resonances are taken into account; the *dashed* line shows the same calculation but without the 'missing' resonance $F_{15}(2000)$.

For example, the π-exchange does not contribute to the beam–target double polarization observables C^{BT}_{ij} in ω photoproduction, making the extraction of individual resonances easier. Figure 3 shows the C^{BT}_{ij} terms which are sensitve to contributions from $F_{15}(2000)$ but cancel out for π-exchange (*dotted lines*). The *solid* curves show the results for the full calculation – based on the quark model approach by Z. Qiao, Z.P. Li, and C. Bennhold – with all resonances included, the *dashed* curves the same calculations without the $F_{15}(2000)$.

Similarly, a set of polarization observables can be determined where contributions of Pomeron exchange[4] are predicted to be vanish.[5]

In order to extract this crucial information we have to study the shape of single and double polarization observables as functions of the c.m. energy W (or photon energy, E_γ) and the production angle $\cos\theta_{cm}$ (or 4-momentum transfer squared, t). The study of observables involving a polarized target is an essential part of this program.[6]

4 Frozen Spin Polarized Target for CLAS

We propose to build a frozen spin target for use in photon-induced experiments with CLAS. The dynamically polarized target used for electron-beam experiments has the disadvantage that is requires the target to be located inside a strong ($\approx$ 5 T) and very uniform (ΔB/B$\approx 10^{-4}$) magnetic field. The magnet needed to produce this field occupies a major fraction of the space around the target sample, leaving only a relatively small acceptance for outgoing particles, and the useful acceptance for low-momentum charged particles may be further reduced by large deflections in the magnetic field. For experiments using a large-aperture spectrometer like CLAS in conjunction with a tagged photon beam, which deposits negligible energy in the target, a more attractive option is to use a frozen spin polarized target.

In a frozen spin target, the material is polarized in the standard way with microwave irradiation in a high magnetic field. Then, with the microwaves off, the temperature of the material is lowered as much as possible, so that the relaxation time of the polarization becomes very long, hence the term "frozen spin". The value of the relaxation time is a strong function of the ratio B/T where B is the value of the magnetic holding field and T the material temperature. By operating at a sufficiently low temperature, it is possible to reduce the holding field to $< 0.5T$ and modest uniformity, while still preserving a high polarization for times acceptable for running the experiment.

The low holding field can be supplied either by the fringe field of the polarizing magnet or by another magnet, the geometry of which can be tailored to the particular experiment to provide a much larger acceptance than obtainable with a high-field magnet. For example, the polarized target for the Bonn–Mainz GDH experiments [42] uses a longitudinal holding field produced by a very

[4]We refer to calculations based on its two-gluon representation following [14].

[5]Due to its imaginary amplitude, observables which are defined as $Im \sum H_i^* H_j$ vanish. See the appendix for details.

[6]A few years ago, when the ω-experiment was launched, we hoped that in a second stage of photoproduction experiments we will make use of the Bonn frozen spin target [41]. Meanwhile, this frozen spin target has become an essential part of the experimental programs at Bonn and Mainz, and will not be available for experiments with CLAS for many years.

thin (500μm) supperconducting solenoid located within the target cryostat which offers virtually no obstruction to the outgoing particles. Another arrangement may be solenoids in a certain distance from the target along the beam axis which do not obstruct the geometrical acceptance of the spectrometer. For transverse polarization, a suitable holding field could be produced by a pair of superconducting Helmholtz coils parallel to the beam axis, also contained within the target cryostat. Figure 4 shows a rough sketch of the holding magnets envisioned for CLAS. The coils could be positioned as much as possible within the shadows of the CLAS torus, to minimize he loss of acceptance.

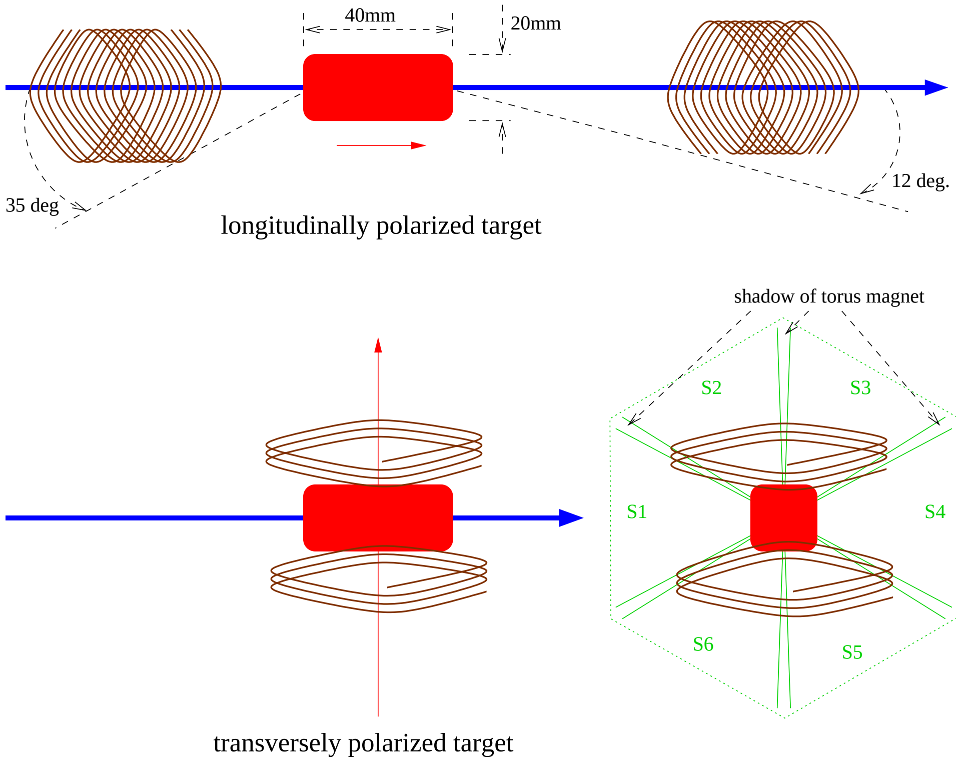

Figure 4: Sketch of the frozen spin target for CLAS.

A “standard” frozen spin target such as the Bonn–target uses butanol as target material. Another possible target material is polyethylene doped with TEMPO, which has similar dilution factor and polarization properties but allows a more accurate measurement of the effective thickness of the target beads. For the purpose of rate calculations, we propose to construct a cylindrical CH_2 target of 40 mm length and 20 mm diamter, with a density of 0.9 g/cm^3 and a free proton density of 0.8×10^{22} protons/cm^3.

A dilution refrigerator is used to provide the lowest temperatures and reasonable cooling power when polarizing. Typical values [43] would be 50 mK for frozen spin operation and 200–400 mK with $\approx$ 50 mW cooling power when polarizing. the University of Virginia (UVa) has the capability of providing such a refrigerator which can be assembled from major components currently in its laboratory. This dilution refrigerator was fabricated at CERN but never assembled; however, three others of the same design have been used very successfully in other experiments at the CERN PS and LEAR.

Other typical parameters for the system are [44]:
a 2.5 T polarizing magnet, microwave frequency of 70 GHz to polarize, and a standard Liverpool Q-meter would measure the polarization to a precision of about 3 %. For a butanol target, proton polarizations of about 90 % with hold times of around 200 hours are achievable, while deuteron polarizations for deuterated butanol could reach 50 % with long hold times.

This target system could efficiently be produced by a collaboration between the Jefferson Lab target group and UVa, and – especially if transverse polarizations are accommodated, would be a flexible facility for a wide range of polarization experiments with CLAS.

A Helicity amplitudes and polarization observables

The appendices give a short summary over the helicity formalism, spin matrices, and polarization observables in the photoproduction of vector mesons.

A.1 Helicity amplitudes

As shown in Fig. 5, the four-momenta of the incoming photon, outgoing vector meson, initial (target) and final (recoil) proton are named $\mathbf{k}, \mathbf{q}, \mathbf{p}$, and $\mathbf{p'}$, respectively. The variables in the c.m. system are written as $\mathbf{k} = (\nu, \vec{k})$, $\mathbf{q} = (E_V, \vec{q})$, $\mathbf{p} = (E_p, -\vec{k})$, and $\mathbf{p'} = (E_{p'}, -\vec{q})$. Additionally, the invariant Mandelstam variables are defined as $s \equiv W^2 = (p+k)^2$, $t = (p-p')^2$, and $u = (k-p')^2$.

Photoproduction of vector mesons can be described by means of helicity amplitudes. The formalism reflects the helicity (spin) correlations of incoming and outgoing particles in the c.m

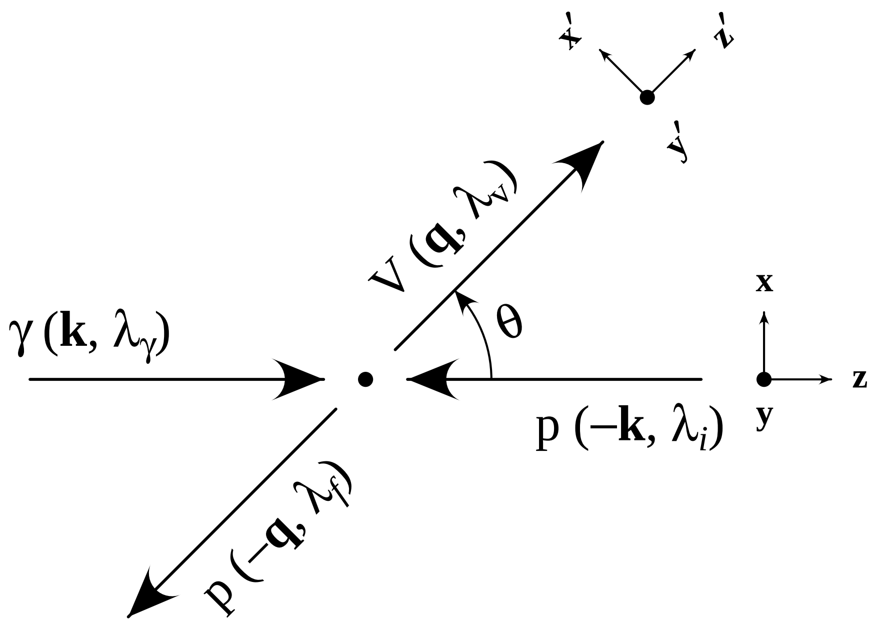

Figure 5: Coordinate system and kinematical variables for photoproduction of vector mesons.

frame. The helicity amplitude has the form

$$H_{\lambda_V,\lambda_f;\lambda_\gamma,\lambda_i} \equiv \langle \mathbf{q};\lambda_V,\lambda_f\,|\,T\,|\,\mathbf{k};\lambda_\gamma,\lambda_i\rangle, \tag{1}$$

where the variables and the coordinate systems are shown in Fig. 5 with λ_γ $(=\pm1)$, λ_V $(=0,\pm1)$, λ_i $(=\pm1/2)$, and λ_f $(=\pm1/2)$ denoting the helicities of the photon, vector meson, target proton, and recoiling proton, respectively. In principle, there are $2\times2\times3\times2=24$ complex amplitudes. However, only 12 complex helicity amplitudes are independent due to parity invariance:

$$\langle \mathbf{q};\lambda_V,\lambda_f|\,T\,|\mathbf{k};\lambda_\gamma,\lambda_i\rangle = (-1)^{\Lambda_f-\Lambda_i}\langle \mathbf{q};-\lambda_V,-\lambda_f\,|\,T\,|\,\mathbf{k};-\lambda_\gamma,-\lambda_i\rangle, \tag{2}$$

with $\Lambda_f=\lambda_V-\lambda_f$ and $\Lambda_i=\lambda_\gamma-\lambda_i$. Following Tabakin *et al.* [17] the 12 independent helicity amplitudes are labeled as

$$\begin{aligned}
H_{1,\lambda_V} &\equiv \langle \lambda_V,\,\lambda_f=+\tfrac{1}{2}\,|\,T\,|\,\lambda_\gamma=1,\,\lambda_i=-\tfrac{1}{2}\rangle,\\
H_{2,\lambda_V} &\equiv \langle \lambda_V,\,\lambda_f=+\tfrac{1}{2}\,|\,T\,|\,\lambda_\gamma=1,\,\lambda_i=+\tfrac{1}{2}\rangle,\\
H_{3,\lambda_V} &\equiv \langle \lambda_V,\,\lambda_f=-\tfrac{1}{2}\,|\,T\,|\,\lambda_\gamma=1,\,\lambda_i=-\tfrac{1}{2}\rangle,\\
H_{4,\lambda_V} &\equiv \langle \lambda_V,\,\lambda_f=-\tfrac{1}{2}\,|\,T\,|\,\lambda_\gamma=1,\,\lambda_i=+\tfrac{1}{2}\rangle.
\end{aligned} \tag{3}$$

The vector-meson photoproduction amplitude can then be represented by a 6×4 matrix $\mathcal{F}$ in helicity space;

$$\mathcal{F} \equiv \begin{pmatrix} H_{2,1} & H_{1,1} & H_{3,-1} & -H_{4,-1} \\ H_{4,1} & H_{3,1} & -H_{1,-1} & H_{2,-1} \\ H_{2,0} & H_{1,0} & -H_{3,0} & H_{4,0} \\ H_{4,0} & H_{3,0} & H_{1,0} & -H_{2,0} \\ H_{2,-1} & H_{1,-1} & H_{3,1} & -H_{4,1} \\ H_{4,-1} & H_{3,-1} & -H_{1,1} & H_{2,1} \end{pmatrix}. \tag{4}$$

In actual calculations, the matrix elements are determined in the nucleon spin space. They are related to the helicity amplitude discussed above, in the reference frame of Fig. 5, by

$$H_{\lambda_V,\lambda_f;\lambda_\gamma,\lambda_i} = (-1)^{1-\lambda_i-\lambda_f} \sum_{m_i,m_f} d^{(1/2)}_{m_i,-\lambda_i}(0) d^{(1/2)}_{m_f,-\lambda_f}(\theta) \langle \lambda_V, m_f \,|\, T \,|\, \lambda_\gamma, m_i \rangle. \tag{5}$$

This expression reduces to that of Ref. [16] for the pseudoscalar meson photoproduction process.

The differential cross section is given by the classical ensemble average as

$$\frac{d\sigma}{d\Omega} = \rho_0 \, \mathrm{Tr}\,(\rho_F). \tag{6}$$

The final state density matrix is

$$\rho_F = \mathcal{F} \rho_I \mathcal{F}^\dagger, \tag{7}$$

where ρ_I is the initial state density matrix,

$$\rho_I = \rho_\gamma \rho_N. \tag{8}$$

The photon and proton density matrices, ρ_γ and ρ_N, are defined below. For example, in the unpolarized case where $\rho_\gamma = \rho_N = \frac{1}{2}$, we get

$$\frac{d\sigma}{d\Omega}^{(U)} = \frac{\rho_0}{4} \, \mathrm{Tr}\,(\mathcal{F}\mathcal{F}^\dagger) \equiv \rho_0 \mathcal{I}(\theta), \tag{9}$$

which defines the cross section intensity $\mathcal{I}(\theta)$.

In general, any spin observable $\bar{\Omega}$ can be written as

$$\bar{\Omega} = \frac{\mathrm{Tr}\,[\mathcal{F} A_\gamma A_N \mathcal{F}^\dagger B_V B_{N'}]}{\mathrm{Tr}\,(\mathcal{F}\mathcal{F}^\dagger)}, \tag{10}$$

where $A_N = (\mathbf{1}_2, \sigma_N)$ and $A'_N = (\mathbf{1}_2, \sigma_{N'})$ which are elements of the nucleon density matrix. The corresponding elements for photon and vector meson are given by $A_\gamma = (\mathbf{1}_2, \sigma_\gamma)$ and $B_V = (\mathbf{1}_3, \Omega^V_j)$.[7] $\mathbf{1}_2$ and $\mathbf{1}_3$ are the 2×2 and 3×3 unit matrices, respectively. Note that the dimensions of the matrices are $\mathcal{F}(6 \times 4)$, $A_\gamma A_N (4 \times 4)$, $\mathcal{F}^\dagger (4 \times 6)$, and $B_V B_{N'} (6 \times 6)$.

[7]One has to use $-\sigma_x$ and $-\sigma_z$ for the initial and final protons instead of σ_x and σ_z in order to have the correct helicity states in the c.m. system [16]. See A.4 for the definition of Ω^V_j.

A.2 Single polarization observables

When only the incoming photon beam is polarized, we can define the polarized beam asymmetry (analyzing power) Σ_x as

$$\Sigma_x = \frac{\mathrm{Tr}\,[\mathcal{F}\sigma_\gamma^x\mathcal{F}^\dagger]}{\mathrm{Tr}\,(\mathcal{F}\mathcal{F}^\dagger)}. \tag{11}$$

If we define $\sigma^{(B,T;R,V)}$ for the cross section $d\sigma/d\Omega$ where the superscripts $(B,T;R,V)$ denote the polarizations of (photon beam, target proton; recoil proton, produced vector-meson), then the physical meaning of Σ_x becomes clear through the relation,

$$\Sigma_x = \frac{\sigma^{(\|,U;U,U)} - \sigma^{(\perp,U;U,U)}}{\sigma^{(\|,U;U,U)} + \sigma^{(\perp,U;U,U)}}, \tag{12}$$

where the superscript U refers to an unpolarized particle and $\|$ $(\perp)$ corresponds to a photon linearly polarized along the $\hat{\mathbf{x}}$ $(\hat{\mathbf{y}})$ axis.

Similarly, we can define the polarized target asymmetry T, recoil polarization asymmetry P, and the vector-meson polarization asymmetry V as

$$\begin{aligned}
T_y &= \frac{\mathrm{Tr}\,(\mathcal{F}\sigma_N^y\mathcal{F}^\dagger)}{\mathrm{Tr}\,\mathcal{F}\mathcal{F}^\dagger)}, \\
P_{y'} &= \frac{\mathrm{Tr}\,(\mathcal{F}\mathcal{F}^\dagger\sigma_{N'}^{y'})}{\mathrm{Tr}\,(\mathcal{F}\mathcal{F}^\dagger)}, \\
V_j &= \frac{\mathrm{Tr}\,(\mathcal{F}\mathcal{F}^\dagger\Omega_j^V)}{\mathrm{Tr}\,(\mathcal{F}\mathcal{F}^\dagger)},
\end{aligned} \tag{13}$$

The explicit expressions for the single polarization observables are given in Appendix A.5.

A.3 Double polarization observables

There are six double polarization observables: Beam–Target (BT), Beam–Recoil (BR), Target–Recoil (TR), Beam–Vector-meson (BV), Target–Vector-meson (TV), and Recoil–Vector-meson (RV). For example, the double polarization observables C_{ij}^{BT} are defined as

$$C_{ij}^{\mathrm{BT}} = \frac{\mathrm{Tr}\,[\mathcal{F}\sigma_\gamma^i\sigma_N^j\mathcal{F}^\dagger]}{\mathrm{Tr}\,(\mathcal{F}\mathcal{F}^\dagger)}. \tag{14}$$

The physical meaning of C_{zz}^{BT} is then

$$C_{zz}^{\mathrm{BT}} = \frac{\mathrm{Tr}\,[\mathcal{F}\sigma_\gamma^z\sigma_N^z\mathcal{F}^\dagger]}{\mathrm{Tr}\,(\mathcal{F}\mathcal{F}^\dagger)} = \frac{\sigma^{(r,z;U,U)} - \sigma^{(r,-z;U,U)}}{\sigma^{(r,z;U,U)} + \sigma^{(r,-z;U,U)}}, \tag{15}$$

where the superscript r corresponds to a circularly polarized photon beam with helicity $+1$, and $\pm z$ denotes the direction of the target proton polarization. Some of the double polarization observables are explicitly given in terms of helicity amplitudes in Appendix A.5. The complete list of double polarization observables can be found in ref. [17].

A.4 Density matrices

In general, the density matrix of the photon can be written as

$$\rho_\gamma = \frac{1}{2}(\mathbf{1}_2 + \sigma_\gamma \cdot \mathbf{P}_S), \tag{16}$$

in the photon helicity space, where $\mathbf{P}_S$ is the Stokes vector which defines the direction and degree of polarization of the photon beam. The presence of σ_γ is due to the fact that a real photon has only two spin degrees of freedom. The Stokes vectors corresponding to some special cases of photon polarization can be found, for example, in Ref. [16].

The proton density matrix is in the spin $\frac{1}{2}$ space and is therefore a 2×2 Hermitian matrix. So we have

$$\rho_N = \frac{1}{2}(\mathbf{1}_2 + \sigma_N \cdot \mathbf{P}_N), \tag{17}$$

for the target proton and

$$\rho_{N'} = \frac{1}{2}(\mathbf{1}_2 + \sigma_{N'} \cdot \mathbf{P}_{N'}), \tag{18}$$

for the recoil proton.

For the vector meson, because of its spin-1 structure, the density matrix cannot be described by vector polarizations only. To describe the vector meson polarization completely, we have to take into account the tensor polarizations. The tensor polarization operator is defined as [33, 34]

$$S_{jk} = \frac{3}{2}(S_j S_k + S_k S_j) - 2\delta_{j\,k}\mathbf{1}_3, \tag{19}$$

where $\mathbf{1}_3$ is the 3×3 unit matrix with

$$S_x = \frac{1}{\sqrt{2}}\begin{pmatrix} 0 & 1 & 0 \\ 1 & 0 & 1 \\ 0 & 1 & 0 \end{pmatrix}, \qquad S_y = \frac{1}{\sqrt{2}}\begin{pmatrix} 0 & -i & 0 \\ i & 0 & -i \\ 0 & i & 0 \end{pmatrix}, \qquad S_z = \begin{pmatrix} 1 & 0 & 0 \\ 0 & 0 & 0 \\ 0 & 0 & -1 \end{pmatrix}. \tag{20}$$

Only five of the elements are independent since $S_{xx} + S_{yy} + S_{zz} = 0$. Therefore, we get to the final form of the density matrix of the vector meson as

$$\rho_V = \frac{1}{3}(\mathbf{1}_3 + \sum_j P_j^V \Omega_j^V), \tag{21}$$

where

$$\Omega_j^V = (\sqrt{\frac{3}{2}}(S_x, S_y, S_z), \quad \frac{1}{\sqrt{6}}(S_{xx} - S_{yy}), \quad \frac{1}{\sqrt{2}}S_{zz}, \quad \sqrt{\frac{2}{3}}(S_{xy}, S_{yz}, S_{zx})), \tag{22}$$

which are normalized as $\mathrm{Tr}\,\Omega_j^V \Omega_k^V = 3\delta_{j\,k}$.

A.5 Single and Double Polarization Observables in Helicity Amplitudes

Among the 290 possible (single, double, triple, and quadruple) polarization observables, only a few of them are explicitly given here in terms of helicity amplitudes, esp. those which involve beam and target polarization.

The cross section intensity $\mathcal{I}(\theta)$ is defined as

$$\mathcal{I}(\theta) = \frac{1}{4}\,\mathrm{Tr}\,(\mathcal{F}\mathcal{F}^\dagger) = \frac{1}{2}\sum_{i=1}^{4}\sum_{a=\pm1,0}|H_{i,a}|^2. \tag{23}$$

The explicit expressions for non-vanishing single polarization observables are as follows.

$$\begin{aligned}
\Sigma_x \cdot \mathcal{I}(\theta) &= -\mathrm{Re}\Big\{H^*_{4,1}H_{1,-1} - H^*_{4,0}H_{1,0} + H^*_{4,-1}H_{1,1} \\
&\qquad - H^*_{3,1}H_{2,-1} + H^*_{3,0}H_{2,0} - H^*_{3,-1}H_{2,1}\Big\}. &(24)\\
T_y \cdot \mathcal{I}(\theta) &= -\mathrm{Im}\,\Big\{H^*_{4,-1}H_{3,-1} + H^*_{4,0}H_{3,0} + H^*_{4,1}H_{3,1} \\
&\qquad + H^*_{2,-1}H_{1,-1} + H^*_{2,0}H_{1,0} + H^*_{2,1}H_{1,1}\Big\}. &(25)\\
P_{y'} \cdot \mathcal{I}(\theta) &= -\mathrm{Im}\,\Big\{H^*_{4,-1}H_{2,-1} + H^*_{4,0}H_{2,0} + H^*_{4,1}H_{2,1} \\
&\qquad + H^*_{3,-1}H_{1,-1} + H^*_{3,0}H_{1,0} + H^*_{3,1}H_{1,1}\Big\}. &(26)\\
V_{y'y'} \cdot \mathcal{I}(\theta) &= -\frac{\sqrt{3}}{2}\mathrm{Im}\,\Big\{H^*_{4,0}(H_{4,1} - H_{4,-1}) + H^*_{3,0}(H_{3,1} - H_{3,-1}) \\
&\qquad + H^*_{2,0}(H_{2,1} - H_{2,-1}) + H^*_{1,0}(H_{1,1} - H_{1,-1})\Big\}. &(27)\\
V_{y'y'x'x'} \cdot \mathcal{I}(\theta) &= \sqrt{\frac{3}{2}}\mathrm{Re}\Big\{H^*_{4,-1}H_{4,1} + H^*_{3,-1}H_{3,1} + H^*_{2,-1}H_{2,1} + H^*_{1,-1}H_{1,1}\Big\}. &(28)\\
V_{z'z'} \cdot \mathcal{I}(\theta) &= \frac{1}{2\sqrt{2}}\Big\{|H_{4,-1}|^2 - 2|H_{4,0}|^2 + |H_{4,1}|^2 + |H_{3,-1}|^2 - 2|H_{3,0}|^2 + |H_{3,1}|^2 \\
&\qquad + |H_{2,-1}|^2 - 2|H_{2,0}|^2 + |H_{2,1}|^2 + |H_{1,-1}|^2 - 2|H_{1,0}|^2 + |H_{1,1}|^2\Big\}. &(29)\\
V_{z'x'} \cdot \mathcal{I}(\theta) &= \frac{\sqrt{3}}{2}\mathrm{Re}\Big\{H^*_{4,0}(H_{4,1} - H_{4,-1}) + H^*_{3,0}(H_{3,1} - H_{3,-1}) \\
&\qquad + H^*_{2,0}(H_{2,1} - H_{2,-1}) + H^*_{1,0}(H_{1,1} - H_{1,-1})\Big\}. &(30)
\end{aligned}$$

The explicit expressions for some double polarization observables are given below.

- Beam–Target

$$\begin{aligned}
C^{\mathrm{BT}}_{yx} \cdot \mathcal{I}(\theta) &= \mathrm{Im}\,\Big\{H^*_{4,-1}H_{2,1} - H^*_{4,0}H_{2,0} + H^*_{4,1}H_{2,-1} \\
&\qquad - H^*_{3,-1}H_{1,1} + H^*_{3,0}H_{1,0} - H^*_{3,1}H_{1,-1}\Big\}, &(31)\\
C^{\mathrm{BT}}_{yz} \cdot \mathcal{I}(\theta) &= -\mathrm{Im}\,\Big\{H^*_{4,-1}H_{1,1} - H^*_{4,0}H_{1,0} + H^*_{4,1}H_{1,-1} \\
&\qquad + H^*_{3,-1}H_{2,1} - H^*_{3,0}H_{2,0} + H^*_{3,1}H_{2,-1}\Big\}, &(32)
\end{aligned}$$

$$
\begin{aligned}
C_{zx}^{\mathrm{BT}} \cdot \mathcal{I}(\theta) &= -\mathrm{Re}\left\{H_{4,-1}^{*}H_{3,-1} + H_{4,0}^{*}H_{3,0} + H_{4,1}^{*}H_{3,1}\right. \\
&\quad \left. + H_{2,-1}^{*}H_{1,-1} + H_{2,0}^{*}H_{1,0} + H_{2,1}^{*}H_{1,1}\right\}, \qquad (33) \\
C_{zz}^{\mathrm{BT}} \cdot \mathcal{I}(\theta) &= -\frac{1}{2}\left\{|H_{4,-1}|^2 + |H_{4,0}|^2 + |H_{4,1}|^2 - |H_{3,-1}|^2 - |H_{3,0}|^2 - |H_{3,1}|^2\right. \\
&\quad \left. + |H_{2,-1}|^2 + |H_{2,0}|^2 + |H_{2,1}|^2 - |H_{1,-1}|^2 - |H_{1,0}|^2 - |H_{1,1}|^2\right\}. \qquad (34)
\end{aligned}
$$

- Beam–Vector-meson

$$
\begin{aligned}
C_{yx'}^{\mathrm{BV}} \cdot \mathcal{I}(\theta) &= -\frac{\sqrt{3}}{2}\mathrm{Im}\left\{H_{4,-1}^{*}H_{1,0} - H_{4,0}^{*}(H_{1,-1} + H_{1,1}) + H_{4,1}^{*}H_{1,0}\right. \\
&\quad \left. - H_{3,-1}^{*}H_{2,0} + H_{3,0}^{*}(H_{2,-1} + H_{2,1}) - H_{3,1}^{*}H_{2,0}\right\}, \qquad (35) \\
C_{yz'}^{\mathrm{BV}} \cdot \mathcal{I}(\theta) &= -\sqrt{\frac{3}{2}}\mathrm{Im}\left\{H_{4,-1}^{*}H_{1,1} - H_{4,1}^{*}H_{1,-1} - H_{3,-1}^{*}H_{2,1} + H_{3,1}^{*}H_{2,-1}\right\}, \qquad (36) \\
C_{zx'}^{\mathrm{BV}} \cdot \mathcal{I}(\theta) &= \frac{\sqrt{3}}{2}\mathrm{Re}\left\{H_{4,0}^{*}(H_{4,-1} + H_{4,1}) + H_{3,0}^{*}(H_{3,-1} + H_{3,1})\right. \\
&\quad \left. + H_{2,0}^{*}(H_{2,-1} + H_{2,1}) + H_{1,0}^{*}(H_{1,-1} + H_{1,1})\right\}, \qquad (37) \\
C_{zz'}^{\mathrm{BV}} \cdot \mathcal{I}(\theta) &= -\frac{1}{2}\sqrt{\frac{3}{2}}\left\{|H_{4,-1}|^2 - |H_{4,1}|^2 + |H_{3,-1}|^2 - |H_{3,1}|^2\right. \\
&\quad \left. + |H_{2,-1}|^2 - |H_{2,1}|^2 + |H_{1,-1}|^2 - |H_{1,1}|^2\right\}. \qquad (38)
\end{aligned}
$$

- Target–Vector-meson

$$
\begin{aligned}
C_{xx'}^{\mathrm{TV}} \cdot \mathcal{I}(\theta) &= -\frac{\sqrt{3}}{2}\mathrm{Re}\left\{H_{4,0}^{*}(H_{3,-1} + H_{3,1}) + H_{3,0}^{*}(H_{4,-1} + H_{4,1})\right. \\
&\quad \left. + H_{2,0}^{*}(H_{1,-1} + H_{1,1}) + H_{1,0}^{*}(H_{2,-1} + H_{2,1})\right\}, \qquad (39) \\
C_{xz'}^{\mathrm{TV}} \cdot \mathcal{I}(\theta) &= \sqrt{\frac{3}{2}}\mathrm{Re}\left\{H_{4,-1}^{*}H_{3,-1} - H_{4,1}^{*}H_{3,1} + H_{2,-1}^{*}H_{1,-1} - H_{2,1}^{*}H_{1,1}\right\}, \qquad (40) \\
C_{zx'}^{\mathrm{TV}} \cdot \mathcal{I}(\theta) &= -\frac{\sqrt{3}}{2}\mathrm{Re}\left\{H_{4,0}^{*}(H_{4,-1} + H_{4,1}) - H_{3,0}^{*}(H_{3,-1} + H_{3,1})\right. \\
&\quad \left. + H_{2,0}^{*}(H_{2,-1} + H_{2,1}) - H_{1,0}^{*}(H_{1,-1} + H_{1,1})\right\}, \qquad (41) \\
C_{zz'}^{\mathrm{TV}} \cdot \mathcal{I}(\theta) &= \frac{1}{2}\sqrt{\frac{3}{2}}\left\{|H_{4,-1}|^2 - |H_{4,1}|^2 - |H_{3,-1}|^2 + |H_{3,1}|^2\right. \\
&\quad \left. + |H_{2,-1}|^2 - |H_{2,1}|^2 - |H_{1,-1}|^2 + |H_{1,1}|^2\right\}. \qquad (42)
\end{aligned}
$$

References

[1] D.B. Lichtenberg, Phys. Rev. **178**, 2197 (1969);
R.E. Cutkosky and R.E. Hendrick, Phys. Rev. D **16**, 2902 (1977).

[2] R. Koniuk and N. Isgur, Phys. Rev. D **21**, 1868 (1980);
N. Isgur and G. Karl, Phys. Lett. **72B**, 109 (1977).

[3] S. Capstick and N. Isgur, Phys. Rev. D **34**, 2809 (1986).

[4] S. Capstick and W. Roberts, Phys. Rev. D **47**, 1994 (1993).

[5] S. Capstick and W. Roberts, Phys. Rev. D **49**, 4570 (1994).

[6] S. Capstick, Phys. Rev. D **46**, 1965 (1992);
S. Capstick, Phys. Rev. D **46**, 2864 (1992).

[7] S. Capstick and B.D. Keister, Phys. Rev. D **47**, 860 (1993).

[8] Particle Data Group, EPJ C **3**, 623 (1998).

[9] C.P. Forsyth and R.E. Cutkosky, Z. Phys. C **18**, 219 (1983).

[10] D. Arndt *et al.*, Phys. Rev. D **43**, 2131 (1991).

[11] D.M. Manley and E.M. Saleski, Phys. Rev. D **45**, 4002 (1992).

[12] B. Fraas, Nucl. Phys. B **36**, 191 (1972).

[13] B. Friman and M. Soyeur, LNS/Ph/95-16, CNRS 1995.

[14] P. V. Landshoff and O. Nachtmann, Z. Phys. C **35**, 405 (1987); A. Donnachie and P. V. Landshoff, Nucl. Phys. **B311**, 509 (1988/1989); J. R. Cudell, Nucl. Phys. **B336**, 1 (1990); J.-M. Laget and R. Mendez-Galain, Nucl. Phys. **A581**, 397 (1995).

[15] Q. Zhao, Z.P. Li, and C. Bennhold, Phys. Rev. C **58**, 2393 (1998);
Q. Zhao, Z.P. Li, and C. Bennhold, Phys. Lett. B **436**, 42 (1998).

[16] C. G. Fasano, F. Tabakin, and B. Saghai, Phys. Rev. C **46**, 2430 (1992).

[17] F. Tabakin, Nucl. Phys. **A570**, 311c (1994); M. Pichowsky, Ç. Şavkli, and F. Tabakin, Phys. Rev. C **53**, 593 (1996).

[18] Ç. Şavklı, F. Tabakin, and S. N. Yang, Phys. Rev. C **53**, 1132 (1996).

[19] F.J. Klein, Ph.D. thesis, Bonn-IR-96-008 (1996);
F.J. Klein, "Overview over Vector Meson Photoproduction," πN Newsletters, No. 14, 141 (1998).

[20] H. Funsten *et al.*, E91-024; V.D. Burkert, "Electromagnetic Excitation of Nucleon Resonances," CEBAF-PR-94-005, (cf. Table 1 for the N^* program).

[21] P.L. Cole, J.P. Connelly, R.R. Whitney, spokespersons, "Photoproduction of ρ Mesons from the Proton with Linearly Polarized Photons," Jefferson Lab E94-109.

[22] P.L. Cole, J.A. Mueller, D.J. Tedeschi, spokespersons, "Photoproduction of ϕ Mesons with Linearly Polarized Photons," Jefferson Lab E98-109.

[23] F.J. Klein, P.L. Cole, spokespersons, "Photoproduction of ω Mesons off Protons with Linearly Polarized Photons," Jefferson Lab E99-013.

[24] R.L. Anderson *et al.*, Phys. Rev. D, 679 (1976).

[25] R.W. Clift *et al.*, Phys. Lett. B **64**, 213 (1976).

[26] Aachen-Berlin-Bonn-Hamburg-Heidelberg-München Collaboration, Phys. Rev. **175**, 1669 (1968).

[27] CEA-Bubble-Chamber-Group, Phys. Rev. **146**, 994 (1966).

[28] Y. Eisenberg *et al.*, Phys. Rev. Lett. **22**, 669 (1969).

[29] J. Ballam *et al.*, Phys. Rev. Lett. **24**, 960 (1970); J. Ballam *et al.*, Phys. Rev. D **7**, 3150 (1973).

[30] Atkinson *et al.*, Nucl. Phys. B **231**, 15 (1984).

[31] G. Fischer *et al.*, Nucl. Phys. B, 93 (1970).

[32] D.P. Barber *et al.*, Z. Phys. C **2**, 1 (1979).

[33] C. Bourrely, E. Leader, and J. Soffer, Phys. Rep. **59**, 95 (1980).

[34] H. E. Conzett, Rep. Prog. Phys. **57**, 1 (1994).
5M. Jacob and G. C. Wick,

[35] M. Pichowsky, C. Savkli, and F. Tabakin, Phys. Rev. C **53**, 593 (1996); C. Savkli, F. Tabakin, and S.N. Yang, Phys. Rev. C **53**, 1132 (1996); W.M. Kloet, W.T. Chiang, and F. Tabakin, Eprint nucl-th/9803042 (1998).

[36] M. A. Pichowsky and T.-S. H. Lee, Phys. Lett. B **379**, 1 (1996); Phys. Rev. D **56**, 1644 (1997).

[37] H. Fraas and D. Schildknecht, Nucl. Phys. **B14**, 543 (1969).

[38] H. J. Besch, G. Hartmann, R. Kose, F. Krautschneider, W. Paul, and U. Trinks, Nucl. Phys. **B70**, 257 (1974).

[39] G. Wolf, Phys. Rev. **182**, 1538 (1969).

[40] A. I. Titov and Y. Oh, Phys. Lett. B **422**, 33 (1998).

[41] W. Meyer, H. Dutz, B. Schoch, *private communication.*

[42] W. Meyer, in *Proceedings of the GDH2000 Symposium* Mainz, Germany, 2000, (World Scientific, 2001) p. 157.

[43] D.G. Crabb and W. Meyer, Ann. Rev. Nucl. Part. Sci. **47**, 67 (1997).

[44] H. Dutz *et al.* , NIM **A356**, 111 (1995).